Karaj branch

Journal of A p p l ied C hemical R esearch
jacr.kiau.ac.ir

Journal of Applied Chemical Research, 18, 3, 86-101 (2024)

Investigation of Fe-Cu-Sr/ γ-Al_2O_3 catalyst performance in Fisher- Tropsch synthesis: Pressure effect

Marziyeh Rahimi Mashkaleh[1], Yahya Zamani[*2], Sahar Baniyaghoob[1], Ensiyeh Ganji Babakhani[2]

[1]*Department of Chemistry, Science and Research Branch, Islamic Azad University, Tehran, Iran*

[2]*Gas Research Division, Research Institute of Petroleum Industry, Tehran, Iran*

(Received 02 Mar. 2024; Final revised received 04 Jun. 2024)

Abstract

Fischer-Tropsch synthesis (FTS) is conducted on the catalysts such as Al_2O_3, SiO_2, TiO_2 and ZrO_2 supported with metals like Co, Fe or Ru. While hydrogen to CO ratio is low, the Iron supported catalysts are more useful to produce alkenes, branched hydrocarbons and oxygenates due to Iron's water-gas-shift (WGS) activity. The aim of this article is to produce C_5^+ hydrocarbon product from synthetic gas using Fe-Cu-Sr/ γ-Al_2O_3 nano-sized catalyst. The nano iron-based catalyst was synthesized by wet impregnation method. The synthesized catalyst (18Fe/4Cu/2Sr/ γ-Al_2O_3) was characterized by XRD, BET, ICP, SEM and H_2-TPR techniques. Effect of reaction pressure on the product selectivity and catalyst activity was investigated in CO hydrogenation reaction. The nano catalyst was loaded in a fixed-bed reactor and tested in pressure of 16 and 20 atm, at temperature of 290 ºC, with H_2/CO ratio of 1 and GHSV of 2 $l.h^{-1}.g\ cat^{-1}$. The results demonstrated that with increasing reaction pressure, the CO conversion and C_5^+ selectivity increased from 63.8% and 44.03% to 78.3% and 46.2%, respectively.

Keywords: CO Hydrogenation, Nano iron based catalyst, Reaction Condition, product selectivity.

[*]***Corresponding author:*** *Yahya Zamani, Gas Research Division, Research Institute of Petroleum Industry, Tehran, Iran. Email: yahyazamani@yahoo.com.*

Introduction

Fischer-Tropsch synthesis (FTS) is a set of chemical reactions in which the CO and H_2 mixture produce a set of hydrocarbons such as fuels. This process was discovered in 1913 with collaboration of Franz Fischer and Hans Tropez in Germany[1, 2]. During the FTS, many reactions occur simultaneously. In principle, the reactive molecules CO and H_2 are separated, forming CHx species and bonding together to form hydrocarbons through chain growth[3, 4]. The most desirable reaction is the production of alkanes, which is shown below:

$$(2n + 1)\ H_2 + n\ CO \rightarrow C_nH_{2n}+2 + n\ H_2O$$

In addition to alkanes, adverse reactions lead to the formation of alcohols, and other oxygenated hydrocarbons [5, 6]. Natural gas resources are abundant and cost-effective around the world, it has attracted the attention of the oil and petrochemical communities to conduct vast studies aiming the improvement of FTS performance to provide clean and sustainable fuels and chemicals. Syngas which is produced by partial oxidation of methane, are processed through FTS to produce hydrocarbons, alcohols and waxes. Upgrading of FT products via hydrocracking and isomerization processes are always integrated into GTL to produce further desired products such as gasoline and diesel and to increase their selectivity, [7-11]. Most group VIII transition metals are active in the FTS process, but often, Fe and Co catalysts are used in the industry because of their ability to create desirable and cost-effective long-chain hydrocarbons. Recently, iron-based catalysts have been compared to cobalt-based catalysts due to their advantages such as cheapness and availability of the metal, good resistance to reaction conditions, and high selectivity for olefins and alcohols, which are widely used as chemical raw materials [12-16]. Co catalysts are usually more resistant to water and consequently can conserve their activity at presence of water. However, iron-based catalysts for the water-gas shift (WGS) reaction are more active than cobalt-based catalysts. This is useful for converting syngas from coal or biomass that have a lower H_2/CO ratio. Cobalt catalysts are active in the suitable temperature and H_2/CO ratio, while iron-based catalysts can operate under a wide range of temperature and H_2/CO ratio without significantly increasing CH_4 selectivity[17, 18]. Iron-based catalysts produce more olefinic products and less choice of CH_4 than cobalt-based catalysts. Reports suggest that when iron and cobalt are used together, they simply do not show the added properties of individual metals [19, 20]. One of the practical ways to increase the economic potential of the FTS process is to produce linear alpha-olefins because they are important chemical mediators for surfactants, functional plastics and elastomers and are also used as an additive to improve octane number of fuels[21-23]. Most studies show that catalyst performance is enhanced by promoting with additives such as K, Mn, Cr, Ru, and pt. Among

these promoters, potassium has been used as a promoter in iron catalysts. Potassium can increase catalytic activity in FTS and WGS reactions. Also, Copper is usually added as a chemical promoter to iron-based catalysts in FTS synthesis, which enhances hematite reduction process. The manganese promoter causes very stable activity and high selectivity in the formation of light olefins in iron catalysts. Some other similar metals like Zr, V, Ta, Mo and La, have a positive effect on catalyst activity for CO hydrogenation and WGS activity [24-26]. γ-Al_2O_3, TiO_2 and SiO_2 are the common supports that used to increase the dispersion of Fe particles to stabilize and prevent the activation of active iron phases. However, they have high interaction with Fe precursors, and create a mixed oxide which is rarely reducible regarding to the lower activity. Thus, the interaction between active component and support should be carefully adjusted[27, 28]. In this study, iron-supported γ-Al_2O_3 catalyst was prepared via impregnation method. After characterization by XRD, BET, SEM and H_2-TPR analysis, the catalyst performance was studied in a fixed-bed reactor. Pressure effect was investigated on the product distribution as well as feed conversion in the FT reaction.

Experimental

Materials and Methods

Catalyst preparation

Nano-sized iron-based catalysts were prepared by wet impregnation method. The preparation process included dissolving 9.12g of Fe $(NO_3)_3.9H_2O$ and 1.06g of Cu $(NO_3)_2.4H_2O$ in deionized water and then adding 0.34g of $Sr(NO_3)_2$ as the promoter. The solution was added to 5.32g of nano γ-Al_2O_3 support in two steps. The sample was dried in an oven at 120 °C for 16 hours and then calcined at 400 °C for 3 hours. The fresh catalyst was sieved to particles with diameters of 250–300 μm.

Catalyst characterization

Brunauer –Emmett–Teller (BET) surface area, pore volume and mean pore size of the catalyst were determined by N_2 physisorption using a Micromeritics ASAP 3020 automated system.

An XRD spectrum of fresh catalyst was conducted with a Philips PW1840 X-ray diffractometer with monochromatized Cu (Kα) radiation to determine the catalyst phase.

Morphology of the calcined catalyst was investigated by the Phenon scanning electron microscopy (SEM).

Temperature-Programmed Reduction of H_2 (H_2-TPR) is based on passage of the reducing gas (hydrogen) through the sample and the reaction with its structural oxygen during heating

operation of the sample. The TPR evaluations of the calcined catalyst was done by a Micromeritics TPD-TPR 290 system. For 50 mg of catalyst, the TPR was conducted in a 5% H_2-95% Ar gas mixture. The catalyst was heated up to 900 from 50 °C at a temperature rate of 10 °C/min. Typically, fresh catalyst was placed in a U-shaped quartz tube and was then heated under diluted H_2 atmosphere under heating. The consumption of H_2 was sensed by thermal conductivity detector [29].

Finally, the amount of hydrogen consumed can be plotted in terms of temperature. To confirm the elemental content of prepared catalysts, digested catalysts were analyzed in a Perkin Elmer Optima 8000 DV ICP analyzer.

Catalyst activity test

As shown in Figure 1, the experiments were carried out at different pressures in a fixed-bed reactor with an inner diameter of 0.95 cm and a length of 75 cm under Fischer-Tropsch synthesis conditions. The catalyst (2 gr) was loaded to the reactor and reduced at 400 °C and atmospheric pressure by a 20% H_2-80% N_2 mixed gas for 2.5 h. The heat required for the reaction is supplied by a three-zone furnace equipped with a temperature controller. The carbide stage was performed in a stream of synthesis gas with H_2 to CO ratio of 1 for 23 h at atmospheric pressure at 270 °C. Then, pressure of the reactor was kept 16 and 20 bar and temperature raised to 290 °C and the reaction was conducted with synthesis gas as feed stream with H_2/CO = 1 and GHSV of 2 l/(h·g).

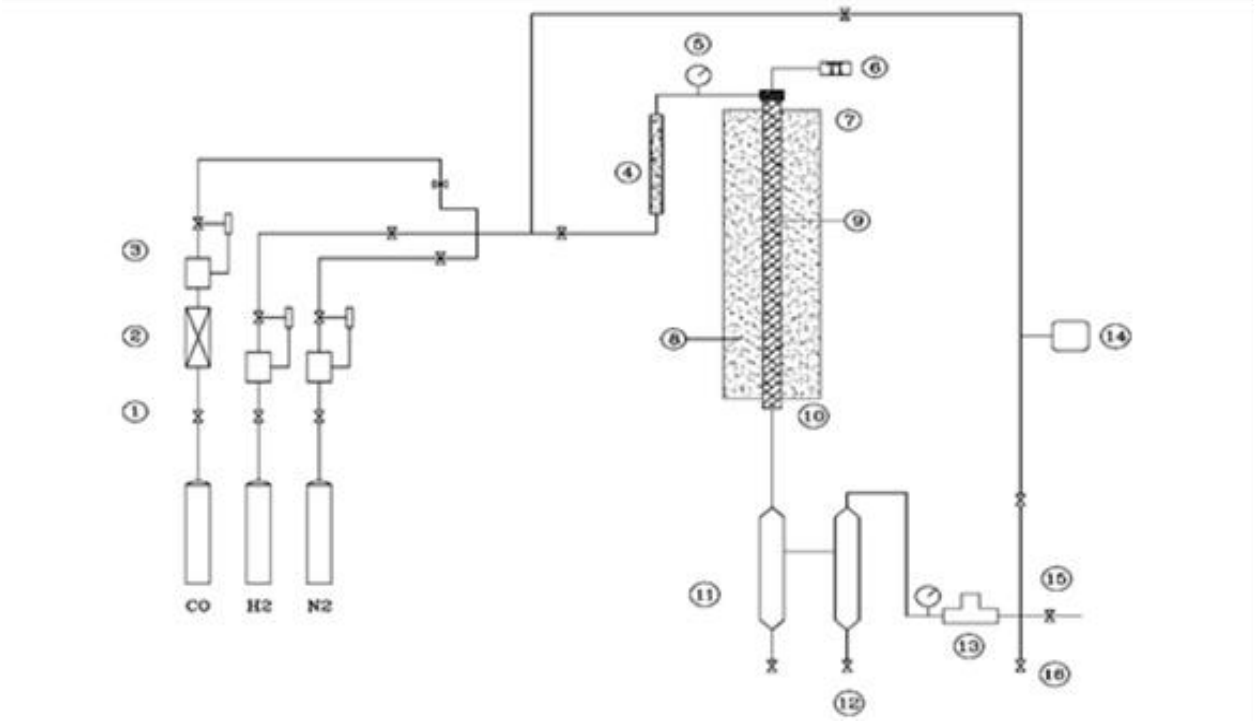

Figure 1. Schematic diagram of experimental set up: (1) Valve, (2) Carbonyl Trap, (3) Mass flow controller, (4) Stationary Mixer, (5) Pressure Regulator, (6) Temperature Indicator, (7) Reactor, (8) Electrical Jacket, (9) (Sic) carborundum, (10) Catalyst, (11) Hot trap, (12) Cold trap, (13) Back pressure Regulator, (14) Gas Chromatography, (15) Flowmeter, (16) Vent.

Results and discussion

After the calcination process, the catalyst was characterized using XRD, BET, SEM, H2-TPR and ICP techniques.

Power X-Ray analysis

XRD patterns of the prepared catalyst was shown in Fig 2. From the XRD results, catalyst phases, and according to the reference articles and JCPDS database, the type of element in the catalyst can be determined and also size of the particles can be calculated [28]. In the prepared catalyst, Fe and γ-Al_2O_3 were used above 10 wt%. As the figure, it can be seen the distinct peaks at 2θ equal to 24.3°, 33.3°, 35.8°, 40.8°, 49.6°, 54.1°, 57.6° and also 64.1° which are related to hematite and 66.5° and 46.1° are related to γ-alumina. This proves the presence of the two phases according to the peaks that appear and Considering that no peaks from other oxides appear, it indicates that the active component of the catalyst is Fe_2O_3[30]. Since the amount of promoter in the catalyst is very small, no related peaks appear and only prevents particles from sticking together with the support-metal interaction [1, 24, 31, 32].

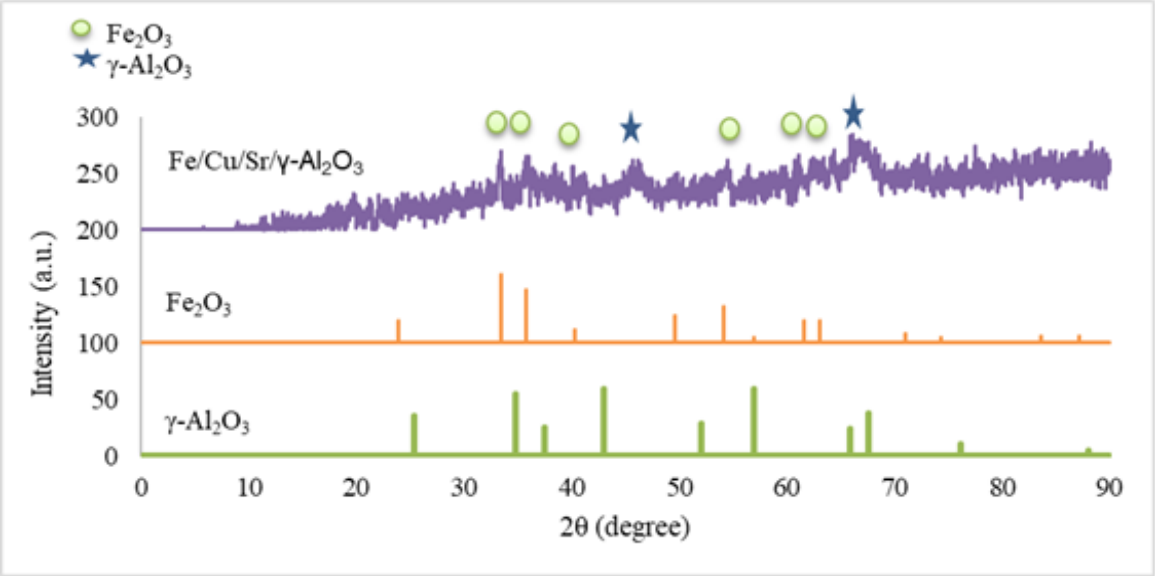

Figure 2. XRD pattern of the catalyst.

XRD pattern indicates the average particle size. In addition, the average particle size can also be obtained by the Debye-Scherrer equation, $d = k\lambda/\beta(\theta)\text{Cos}\theta$, from the peak width in a wide angle X-ray scattering (WAXS) measurement of the material, where λ is the X-ray wavelength (nm), $\beta(\theta)$ is the full width at half maximum (rad) of the identified peak, θ is the diffraction angle, and k is the typical constant of the equipment. Particle size of the catalyst is caculated 32nm.

Surface area analysis of calcined samples

Surface area, pore volume and pore size of the catalyst determined from the BET analysis are shown in Table 1.

Table 1. Textural properties of fresh catalysts.

Catalyst System	Surface Area (m^2/g)	Average pore size (A °)	Pore Volum (cm^3/g)
γ-Al_2O_3	207.6	131.5	0.68
18Fe/4Cu/2Sr/ γ-Al_2O_3	156.3	99.7	0.39

According to the results obtained from BET, the promoter decreased surface area and pore volum of the catalyst because of blocking support cavities [31]. Al_2O_3 increases the area of iron catalysts[33]. The Fe/γ-Al_2O_3 catalyst has a high surface area. The addition of Sr and Cu to the catalyst decreased the BET surface area and pore volume, indicating that these metals

were effectively introduced into the porous structure of the catalyst. This reduction may be due to the formation of larger hematite crystals[34]. The pore size of the γ- Al_2O_3 supported catalyst was determined by N_2 adsorption-desorption measurement shown in fig.3. As this Figure, the obtained isotherm is type IV with an H_2-type hysteresis loop (according to Brunauer-Deming-Deming-Teller classification (BDDT)), which is a characteristic feature of mesoporous structure. The hysteresis loop is caused by the occurrence of capillary condensate[35].

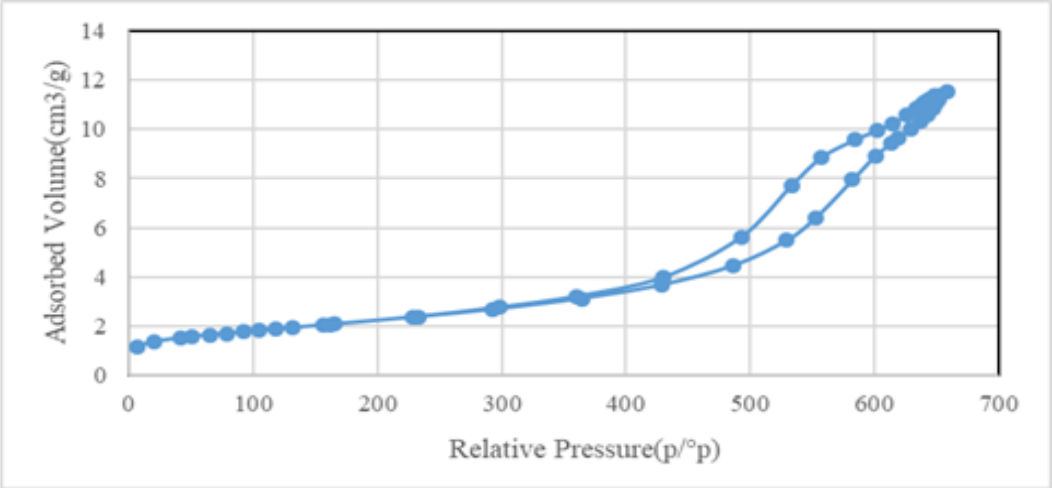

Figure 3. Nitrogen absorption and desorption of the 18Fe/4Cu/2Sr/ γ-Al_2O_3 catalyst

Scaning Electron Microscopy

SEM image of the prepared alumina-supported iron catalyst is presented in fig. 4 that gave information about the morphology and particle size of the catalyst. In fig.5 particle size distribution of the prepared catalyst is shown. According to SEM image, the particle size is about 10 - 80 nm and the dispersion of the active particles on the alumina support is well done. In addition, it can be observed particles of the catalyst were uniformly distributed on the support.

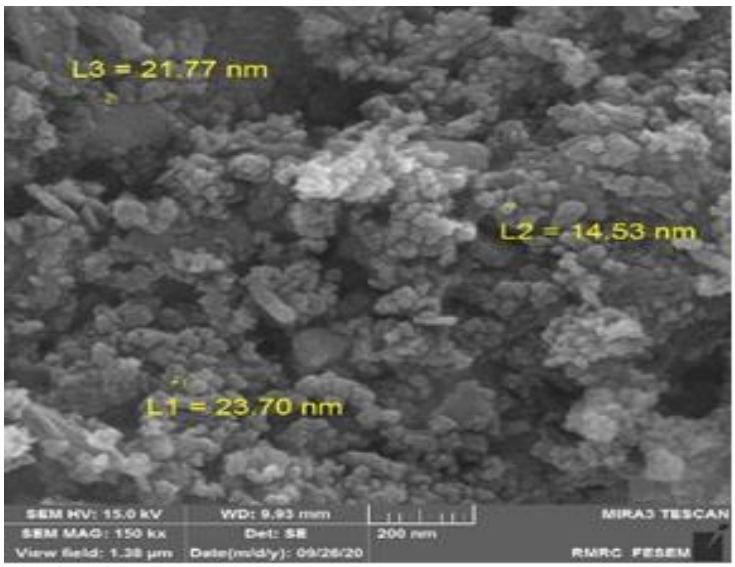

Figure 4. SEM image of the 18Fe/4Cu/2Sr/ γ-Al_2O_3 catalyst.

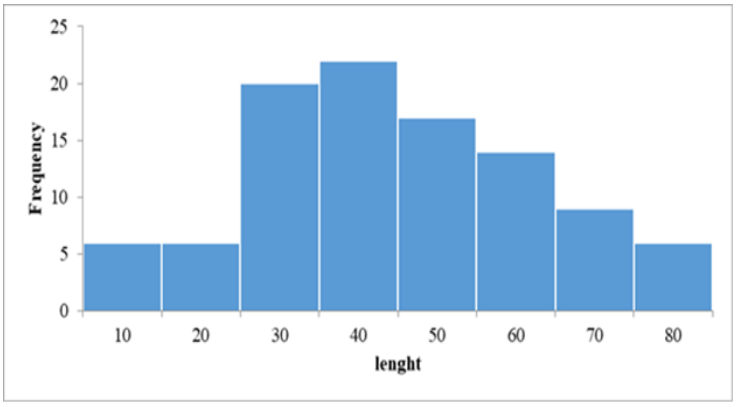

Figure 5. Histogram for the 18Fe/4Cu/2Sr/ γ-Al_2O_3 catalyst.

Inductively Coupled Plasma−Atomic Emission Spectrometer analysis

The quantities of loaded promoters on the catalysts were measured using ICP-OES and are presented in Table 3. As seen in the table, the measured amount of the elements were relatively close to the caculated theoretical one. The results show that the read values are consistent with the theoretical content.

Table 3. Compositions of the samples determined by ICP.

Catalyst	Al %	Fe %	Cu %	Sr %	Ce %
18Fe/4Cu/2Sr/γ-Al_2O_3	34.8	17.4	3.7	1.9	-

H_2-Temperature programmed reduction

Figure 6 is related to the reduction profile of the calcined powder catalyst and shows different reduction peaks and provides useful information on the dispersion of supported iron oxide

phases. The H_2-TPR profiles displayed hydrogen consumption peaks from Fe_2O_3 hematite to metallic iron.

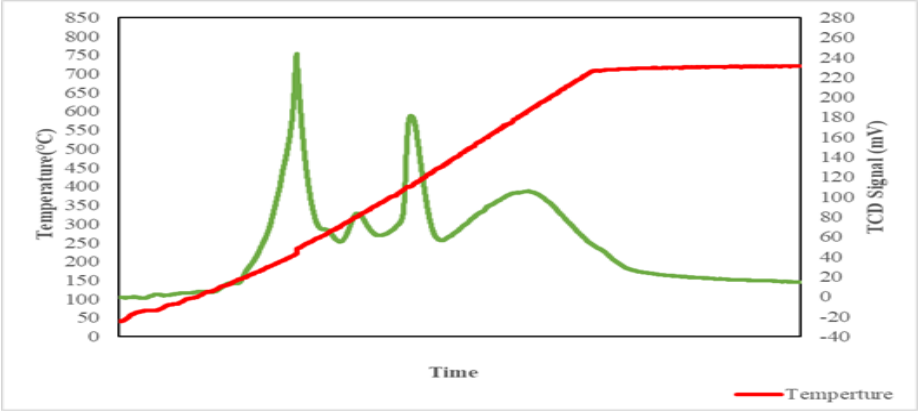

Figure 6. H_2-TPR profile of the18Fe/4Cu/2Sr/ γ-Al_2O_3 catalyst.

The first peak is attributed to the reduction of CuO to Cu, the second peak is related to the reduction of Fe_2O_3 to Fe_3O_4 and third peak is related to the reduction of Fe_3O_4 to Fe. The reduction of Fe_3O_4 to Fe depends on the particle size and the interaction with the structural promoters. Table 2 shows the quantitative results of H_2 consumption for the fresh catalyst in H_2-TPR analysis.

Table 2. Quantitative results of H_2 consumption for the 18Fe/4Cu/2Sr/ γ-Al_2O_3 catalyst.

Catalyst	**Temp(°C)**	**H_2 consumption**	
		mmole H_2	**mmole H_2/g**
Fe/Cu/Sr/γ-Al_2O_3	226.9	0.08	2.36
	407.5	0.12	3.54

Amount of the hydrogen consumption in the first step is related to the reduction of CuO and FeO, and the amount of hydrogen consumption at a temperature of 400 °C is related to the reduction of FeO to Fe. The results showed that the incorporation of Cu and Sr in the iron-based catalyst increases the absorption rate of H_2 and facilitates the reduction of the iron-based catalyst[36].

Reactor system and product analysis

In Table 3, the effect of pressure on the selectivity of products over Fe-Cu catalysts during the FTS reaction is presented. In this table, the selectivity for light hydrocarbons (methane and C_2–C_4), and heavy hydrocarbons (C_5^+) are given. Results showed as pressure increases, formation

of the heavy hydrocarbons increases while hydrogenation reaction is inhibited. In other words, higher pressure leads to lower CH_4 selectivity and higher C_5^+ selectivity.

Also in Table 3, FT performance of the prepared catalyst is compared to that of some typical catalysts in other references. From the table 3, it can be seen that the prepared catalyst has an appropriate performance in the present work in comparison to the previous given results. It can be concluded from the results that operating conditions such as pressure, temperature, space velocity and feed ratio affect significantly on the conversion and selectivity of the products.

Table 3. Comparison of product selectivity of the literature overview catalysts and present work.

Catalyst	P (atm)	T (°C)	H_2/CO	GHSV (l.hr1.gCat-1)	Selectivity				No. references
					C_1	C_2-C_4	C_5^+	CO_2	
Fe/Cu/K	14.8	250	1	2[a]	11.6	30.4	58	48.2	[37]
Fe/Zr/SiO_2	15	270	0.4	1	7.89	24.95	67.16	30.58	[38]
Fe/SiO_2	20	300	2	8	14.6	37.6	47.8	19.1	[39]
Fe/Cu/La	18	290	1	3[a]	12.32	26.19	38.06	23.43	[40]
Fe/Zr	20	250	2	0.008	28	39.4	30.8	5.17	[41]
Fe/SiO_2	20	270	2	N.G.[b]	15	40	33.2	12	[42]
FeAl-Sol	23	200	3	5	3.1	11.9	85	18.1	[29]
FeNi/SiO_2	35	250	0.69	1	17.66	36.17	12.28	39.16	[43]
Fe/Cu/La/Si	17	290	1	5.04[a]	10.3	17.99	44.03	24.62	[44]
Fe/Cu/Sr/γ-Al_2O_3	16	290	1	2	13.36	17.99	44.03	24.62	This work
Fe/Cu/Sr/γ-Al_2O_3	20	290	1	3	11.57	13.73	46.2	28.5	This work

[a] $nl.hr^{-1}.gCat^{-1}$, [b] Not Given, [c] Present work.

Yield and CO conversion obtained from different pressure are presented in Figure 7. Contrary to CH_4 selectivity, higher pressure leads to increase the yield and CO conversion. This is agreement to what is observed in previous studies [45].

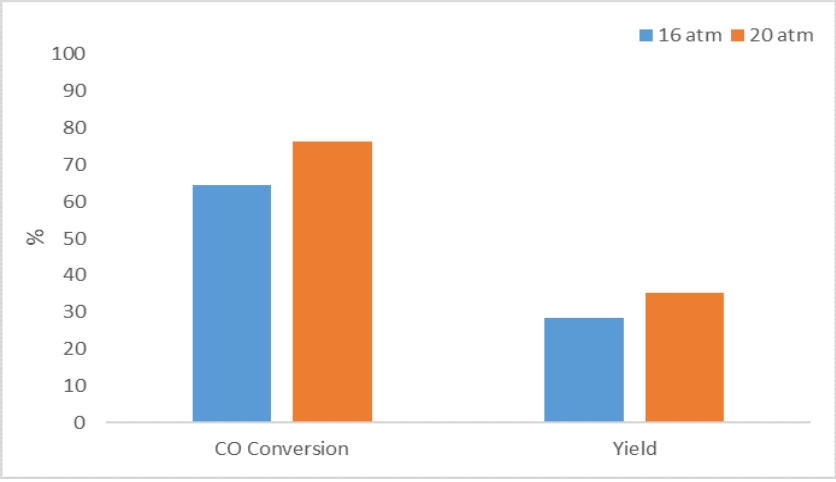

Figure 7. CO conversion and yield of the 18Fe/4Cu/2Sr/ γ-Al2O3catalyst.

Performance of the catalyst during time on stream for two pressures is shown in Figure 8. CO conversion during time on stream decreased because of deactivating small active phase particles.

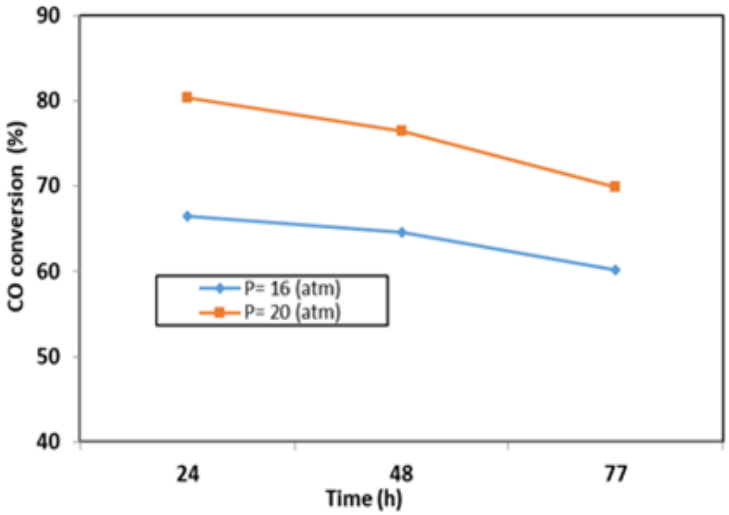

Figure 8. CO conversion and yield of the18Fe/4Cu/2Sr/ γ-Al_2O_3 catalyst.

The results of the reactor tests showed that choosing the appropriate reduction temperature and the amount of hydrogen from the H_2-TPR results play important rule to have a good catalyst performance.

Conclusion

In this work, nano-sized iron catalyst was synthesized through impregnation method. The effect of pressure was investigated on the product distribution of the iron catalyst in Fischer-Tropsch synthesis, it was found that increasing reaction pressure has significant influence on decreasing

methane product of the FTS, which can be related to the decline of H2/CO in the active phase. Increasing pressure caused enhancement of heavy hydrocarbons' yield and CO conversion.

References

1. Pour AN, Shahri SMK, Zamani Y, Zamanian A. Promoter effect on the CO2-H2O formation during Fischer-Tropsch synthesis on iron-based catalysts. Journal of natural gas chemistry. 2010;19(2):193-7.

2. Mandić M, Todić B, Živanić L, Nikačević N, Bukur DB. Effects of catalyst activity, particle size and shape, and process conditions on catalyst effectiveness and methane selectivity for Fischer–Tropsch reaction: a modeling study. Industrial & Engineering Chemistry Research. 2017;56(10):2733-45.

3. Xie J, Yang J, Dugulan AI, Holmen A, Chen D, de Jong KP, et al. Size and promoter effects in supported iron Fischer–Tropsch catalysts: Insights from experiment and theory. ACS Catalysis. 2016;6(5):3147-57.

4. Hadnađev-Kostić MS, Vulić TJ, Marinković-Nedučin RP, Nikolić AD, Jović B. Mg-Fe-mixed oxides derived from layered double hydroxides: a study of the surface properties. Journal of the Serbian Chemical Society. 2011;76(12):1661-71.

5. Kaneko T, Derbyshire F, Makino E, Gray D, Tamura M, Li K. Ullmann's Encyclopedia of Industrial Chemistry, Coal Liquefaction. 2012;10(14356007):a07_197.

6. Stamenić M, Dikić V, Mandić M, Todić B, Bukur DB, Nikačević NM. Multiscale and Multiphase Model of Fixed-Bed Reactors for Fischer–Tropsch Synthesis: Optimization Study. Industrial & Engineering Chemistry Research. 2018;57(9):3149-62.

7. Vosloo AC. Fischer–Tropsch: a futuristic view. Fuel processing technology. 2001;71(1-3):149-55.

8. Almalki FA. Selective Deposition of Platinum by Strong Electrostatic Adsorption onto Cobalt-and Iron-based Catalysts for Fischer-Tropsch Synthesis. 2018 ; Ph.D thesis, College of Engineering and Computing, South Carolina.

9. Chum HL, Overend RP. Biomass and renewable fuels. Fuel processing technology. 2001;71(1-3):187-95.

10. Sharma B, Ingalls RG, Jones CL, Khanchi A. Biomass supply chain design and analysis: Basis, overview, modeling, challenges, and future. Renewable and Sustainable Energy Reviews. 2013;24:608-27.

11. Stamenić M, Dikić V, Mandić M, Todić B, Bukur DB, Nikačević NM. Multiscale and multiphase model of fixed bed reactors for Fischer–Tropsch synthesis: intensification possibilities study. Industrial & Engineering Chemistry Research. 2017;56(36):9964-79.

12. Li X, Liu X, Liu Z-W, Asami K, Fujimoto K. Supercritical phase process for direct synthesis of middle iso-paraffins from modified Fischer–Tropsch reaction. Catalysis Today. 2005;106(1-4):154-60.

13. Zhang Y, Koike M, Yang R, Hinchiranan S, Vitidsant T, Tsubaki N. Multi-functional alumina–silica bimodal pore catalyst and its application for Fischer-Tropsch synthesis. Applied Catalysis A: General. 2005;292:252-8.

14. Geng S, Jiang F, Xu Y, Liu X. iron-based Fischer–Tropsch synthesis for the efficient conversion of carbon dioxide into Isoparaffins. ChemCatChem. 2016;8(7):1303-7.

15. Wei Y, Luo D, Zhang C, Liu J, He Y, Wen X, et al. Precursor controlled synthesis of graphene oxide supported iron catalysts for Fischer–Tropsch synthesis. Catalysis Science & Technology. 2018;8(11):2883-93.

16. Zhang X, Lin Q, Liu B, Zheng J, Jiang F, Xu Y, et al. Unravelling the structure-performance relationship over iron-based Fischer-Tropsch synthesis by depositing the iron carbonyl in syngas on SiO2 in a fixed-bed reactor. Applied Catalysis A: General. 2019;572:197-209.

17. CHEN Y-l, SUN J-q, ZHANG Y-f, ZHENG S-k, WANG B-h, Zheng C, et al. CoFe2O4 nanoarray catalysts for Fischer-Tropsch synthesis. Journal of Fuel Chemistry and Technology. 2017;45(9):1082-7.

18. Kuila D, Nagineni V, Zhao S, Indukuri H, Liang Y, Potluri A, et al. Characterization of alumina and silica sol-gel encapsulated Fe/Co/Ru nanocatalysts in microchannel reactors for FT synthesis of higher alkanes. MRS Online Proceedings Library Archive. 2004;820.

19. Abrokwah RY, Rahman MM, Deshmane VG, Kuila D. Effect of titania support on Fischer-Tropsch synthesis using cobalt, iron, and ruthenium catalysts in silicon-microchannel microreactor. Molecular Catalysis. 2019;478:110566.

20. Ma X, Sun Q, Ying W, Fang D. Effects of promoters on catalytic performance of Fe-Co/SiO2 catalyst for Fischer-Tropsch synthesis. Journal of natural gas chemistry. 2009;18(3):354-8.

21. Yang S, Lee S, Kang SC, Han SJ, Jun K-W, Lee K-Y, et al. Linear α-olefin production with Na-promoted Fe–Zn catalysts via Fischer–Tropsch synthesis. RSC advances. 2019;9(25):14176-87.

22. Jothimurugesan K, Goodwin Jr JG, Gangwal SK, Spivey JJ. Development of Fe Fischer–Tropsch catalysts for slurry bubble column reactors. Catalysis Today. 2000;58(4):335-44.

23. Pour AN, Zamani Y, Tavasoli A, Shahri SMK, Taheri SA. Study on products distribution of iron and iron–zeolite catalysts in Fischer–Tropsch synthesis. Fuel. 2008;87(10-11):2004-12.

24. Li S, Li A, Krishnamoorthy S, Iglesia E. Effects of Zn, Cu, and K promoters on the structure and on the reduction, carburization, and catalytic behavior of iron-based Fischer–Tropsch synthesis catalysts. Catalysis Letters. 2001;77(4):197-205.

25. Duvenhage D, Coville N. Effect of K, Mn and Cr on the Fischer–Tropsch activity of Fe: Co/TiO 2 catalysts. Catalysis letters. 2005;104(3):129-33.

26. Zamani Y, Zamaniyan A, Bahadoran F, Shojaei M. Effect of calcium promoter on nano structure iron catalyst for Fischer–Tropsch synthesis. Journal of Petroleum Science and Technology. 2015;5(1):21-7.

27. de Smit E, Weckhuysen BM. The renaissance of iron-based Fischer–Tropsch synthesis: on the multifaceted catalyst deactivation behaviour. Chemical Society Reviews. 2008;37(12):2758-81.

28. Zhao X, Lv S, Wang L, Li L, Wang G, Zhang Y, et al. Comparison of preparation methods of iron-based catalysts for enhancing Fischer-Tropsch synthesis performance. Molecular Catalysis. 2018;449:99-105.

29. Chou W, Wu P, Luo M, Li W, Li S. Effects of Al, Si, Ti, Zr Promoters on Catalytic Performance of Iron-Based Fischer–Tropsch Synthesis Catalysts. Catalysis Letters. 2020;150(7):1993-2002.

30. Chou W, Wu P, Luo M, Li W, Li S. Effects of Al, Si, Ti, Zr promoters on catalytic performance of iron-based Fischer–Tropsch synthesis catalysts. Catalysis Letters. 2020;150:1993-2002.

31. Jongsomjit B, Panpranot J, Goodwin Jr JG. Co-support compound formation in alumina-supported cobalt catalysts. Journal of Catalysis. 2001;204(1):98-109.

32. Pour AN, Shahri SMK, Bozorgzadeh HR, Zamani Y, Tavasoli A, Marvast MA. Effect of Mg, La and Ca promoters on the structure and catalytic behavior of iron-based catalysts in Fischer–Tropsch synthesis. Applied Catalysis A: General. 2008;348(2):201-8.

33. Pengnarapat S, Ai P, Reubroycharoen P, Vitidsant T, Yoneyama Y, Tsubaki N. Active Fischer-Tropsch synthesis Fe-Cu-K/SiO2 catalysts prepared by autocombustion method without a reduction step. Journal of energy chemistry. 2018;27(2):432-8.

34. Sudsakorn K, Goodwin JG, Jothimurugesan K, Adeyiga AA. Preparation of attrition-resistant spray-dried Fe Fischer− Tropsch catalysts using precipitated SiO2. Industrial & engineering chemistry research. 2001;40(22):4778-84.

35. Yaghoobpour E, Zamani Y, Zarrinpashne S, Zamaniyan A. Fischer–Tropsch synthesis: effect of silica on hydrocarbon production over cobalt-based catalysts. Chemical Papers. 2019;73:205-14.

36. Jabalameli M, Zamani Y, Baniyaghoob S, Shirazi L. Investigation of Mn and Ca promoter effects in iron-based catalysts: CO hydrogenation reaction. New Journal of Chemistry. 2023;47(20):9923-32.

37. Wan H, Wu B, Zhang C, Xiang H, Li Y. Promotional effects of Cu and K on precipitated iron-based catalysts for Fischer–Tropsch synthesis. Journal of Molecular Catalysis A: Chemical. 2008;283(1-2):33-42.

38. Zhang H, Ma H, Zhang H, Ying W, Fang D. Effects of Zr and K promoters on precipitated iron-based catalysts for Fischer–Tropsch synthesis. Catalysis letters. 2012;142(1):131-7.

39. Aluha J, Braidy N, Dalai A, Abatzoglou N. Low-temperature Fischer-Tropsch synthesis using plasma-synthesized nanometric Co/C and Fe/C catalysts. The Canadian Journal of Chemical Engineering. 2016;94(8):1504-15.

40. Zamani Y, Bakavoli M, Rahimizadeh M, Mohajeri A, Seyedi SM. Synergetic effect of La and Ba promoters on nanostructured iron catalyst in Fischer-Tropsch synthesis. Chinese Journal of Catalysis. 2012;33(7-8):1119-24.

41. Aldossary MAM. Structure and reactivity of iron-based catalysis for Fischer-Tropsch synthesis. 2015.

42. Zamani Y, Mohajeri A, Bakavoli M, Rahimizadeh M, SEYEDI SM. The Effect of Temperature on Product Distribution over Fe-Cu-K Catalyst in Fischer-Tropsch Synthesis. 2016; 6(1), 46-52

43. Qian W, Zhang H, Sun Q, Liu Y, Ying W, Fang D. Effects of Zr and Ni promoters on the activation and deactivation of a precipitated iron-based catalyst for Fischer–Tropsch synthesis. Reaction Kinetics, Mechanisms and Catalysis. 2014;111(1):293-304.

44. Pour AN, Zare M, Shahri SMK, Zamani Y, Alaei MR. Catalytic behaviors of bifunctional Fe-HZSM-5 catalyst in Fischer–Tropsch synthesis. Journal of Natural Gas Science and Engineering. 2009;1(6):183-9.

45. Niu C, Xia M, Chen C, Ma Z, Jia L, Hou B, et al. Effect of process conditions on the product distribution of Fischer-Tropsch synthesis over an industrial cobalt-based catalyst using a fixed-bed reactor. Applied Catalysis A: General. 2020;601:117630.